Dispersion tailored suspended core SiN channel waveguide for broadband supercontinuum generation

Mohammed Faisal[a,], M. R. Karim[a], Taqui Shafiq[a], B. M. A. Rahman[b]

[a]*Department of Electrical and Electronic Engineering, Chittagong Independent University, Chattogram, Bangladesh*
[b]*Department of Electrical and Electronic Engineering, City University of London, UK*

Abstract

Integrated photonics have been growing at a exponential rate. The related technologies are advancing with plethora of research works on intergrated devices offering Complementary Metal-Oxide-Semiconductor (CMOS) compatibility. Various compact waveguides are also exploited for different applications. In this paper, we report a novel on-chip CMOS compatible 5 mm long air-clad SiN suspended core channel waveguide. The rectangular core is suspended on a Silicon Nitride slab with the lower cladding on which the slab rests upon is a hollowed-out Silica (SiO_2) rectangular substrate. The proposed waveguide is designed to be numerically pumped at 1.55 μm wavelength with a pulse having a 20 kW power and a temporal width of 50 fs. Supercontinuum coverage ranging from 0.8 μm to 6 μm is observed, which can be utilized in various applications such as spectroscopy, optical coherence tomography, and bio-medical imaging.

Keywords: Suspended core waveguide, SiN waveguide, Dispersion, Nonlinearity, SC generation

1. Introduction

Integrated photonics have attracted great attention in the recent past due to its vast applications in a multitude of arenas. To be precise, the supercontinuum generation (SCG) has acted as the catalyst to this revolution. Supercontinuum (SC) is simply the broadband spectrum obtained due to the interplay between linear and nonlinear effects in a waveguide. This high intensity light with broad spectrum find applications in spectroscopy, imaging, optical communications and frequency metrology. In Spectroscopy the SC provides a broadband light source, which is absorbed by various chemical species at certain frequency bands. This is utilized by the spectrometer in identification of the presence of a particular chemical compound [1]. SCG also contributes to imaging where broad and coherent spectra leads to high resolution images [2]. Frequency combs which are a close entity to SCG are finding great importance in the recent times where Wavelength Division Multiplexing (WDM) can be utilized for optical communications [3].

Planar waveguides, channel waveguides, and optical fiber are the three types of optical waveguides [4]. Many texts consider optical fibers to be channel waveguides [5], but due to their widespread use, they can be treated as a separate entity. Planar waveguides are rectangular channel waveguides that include the ridge or wire waveguide, the rib waveguide, and the slot waveguide [4]. SCG employs both channel waveguides and optical fibers. However, due to their compact size, ease of fabrication, and Complementary Metal-Oxide-Semiconductor (CMOS) integration capability, planar waveguides are preferred for SCG over optical fibers [6].

Channel waveguides have been extensively studied numerically and experimentally in the recent past. Choice of material and geometrical variation in the waveguide design for dispersion engineering are the main key aspects of the analysis conducted for broad SCG. Materials including Silicon, Germanium (Ge) [7], Silicon-Germanium (SiGe), Silicon Nitride (SiN), SF57 [8], Lithium Niobate ($LiNbO_3$) [9] and Chalcogenide glasses [10, 11, 12] have found eminent importance in the waveguide design. Silicon in the form of Silicon-on-Insulator (SOI) has been extensively

*Corresponding author
Email address: mrkarim@ciu.edu.bd (M. R. Karim)

analyzed in the past. Neetesh *et al.* experimentally generated a coherent supercontinuum spanning from 1.06 μm to 2.40 μm with a bandwidth of -20 dB in a SOI ridge waveguide employing a pump source of 100 fs duration with 18 pJ energy at 1.9 μm wavelength [13]. Ryan *et al.* experimentally generated a SC ranging from 1.51 μm to 3.67 μm in a silicon wire waveguide pumped at 2.5 μm wavelength with 300 fs pulses having a peak power of 125 W [14]. Another platform, Silicon-on-Sapphire (SOS) was utilized by Neetesh *et al.* to demonstrate a SC ranging from 1.9 μm to 6 μm pumping at a wavelength of 3.7 μm [15]. Other cases were also reported where SOS was utilized [16]. Another candidate, SiGe waveguide attracted great attention due to the transparency limit of Germanium which is up to 14.5 μm [17]. Alberto *et al.* experimentally pumped a SiGe waveguide with 200 fs pulse at a wavelength of 4.6 μm to obtain a SC from 3.39 μm to 6.02 μm [18]. Sinobad *et al.* experimentally pumped a SiGe-on- Silicon waveguide with a 200 fs pump pulse generating a 2.8 μm to 5.7 μm SC [19]. Although Si-on-Sapphire and SiGe-on-Si presented a broad spectrum, they have drastic drawbacks which backlashes their use. The lattice mismatch between Silicon, Germanium and Sapphire increases the propagation loss of the waveguide to a high degree in terms of integrated photonics. On the other hand, although Silicon presents great application owing to high Kerr coefficient, large index difference and mature fabrication, it can seldom be used to generate SC extending in the Mid-Infrared (MIR) region [20, 21]. This is because Silicon suffers from high Two Photon Absorption (TPA) and Free Carrier Absorption (FCA) in the telecom wavelength and also experiences Three Photon Absorption (3PA) above 2.5 μm wavelength. Hence focus has been shifted towards other materials which can overcome the obstacles. Chalcogenide glasses has gained immense popularity in optical fibers and is also finding some place in the channel waveguides [22]. However, the chalcogenide materials are not fit for large and low cost production of compact on-chip devices due to their incompatibility with CMOS technology [23]. Silicon Nitride (SiN) on the other hand is one such material which has attracted great attention owing to its supremacy over Silicon. Low index contrast, low loss, negligible TPA in the telecom wavelength, low thermo optic coefficient and manufacturing flexibility has kept SiN a step ahead especially for broad SC generation [20, 24]. Extensive research works have been performed in the recent past where waveguides employing SiN as core has been analyzed and hence dispersion engineered for broadband SC generation [25]. Zhao *et al.* [26] experimentally generated a SC ranging from 488 nm to 978 nm in a under-etched Si_3N_4 waveguide utilizing a pump with 874 W power and 100 fs duration at a wavelength of 795 nm. They also conducted numerical analysis which were in good agreement with the experimental results. Johnson *et al.* [27] experimentally generated a SC in a Si_3N_4 waveguide extending from 673 nm to 1944 nm using a pump with 437 pJ pulse energy and 92 fs duration at a wavelength of 1030 nm. Numerical analysis conducted also were in good hand with the experiments. Liu *et al.* [28] experimentally and numerically generated a SC in a Silicon-Rich Nitride waveguide starting from 820 nm and ending to about 2250 nm using a pump with 105 fs pulse duration at a wavelength of 1555 nm. Christian *et al.* [23] experimentally and numerically generated an ultrabroadband supercontinuum covering two octaves, comprising the visible and near-infrared wavelength ranges using a N-Rich Silicon Nitride waveguide employing a pump of 0.56 nJ pulse energy and 130 fs duration at a wavelength of 1200 nm. Marco *et al.* [29] experimentally generated a SC spanning from 526 nm to 2600 nm in a stoichiometric Si_3N_4 waveguide employing a pump source with 300 mW average power and 120 fs pulse duration pumped at a wavelength of 1560 nm. They also conducted numerical analysis which were in good agreement with the experimental results. Hairun *et al.* [30] experimentally and numerically generated a SC in a Si3N4 waveguide starting from 560 nm and ending to about 3600 nm using a pump with pulse duration less than 90 fs and average power less than 110 mW at a wavelength of 1500 nm. Grassani *et al.* [31] experimentally and numerically generated a SC in a SiN waveguide starting from 500 nm and ending to about 3600 nm using a pump with 4.2 kW power and 130 fs duration at a wavelength of 1550 nm. A broader SC spanning from 1200 nm to 3700 nm was experimentally demonstrated in a Si_3N_4 waveguide by Martyshkin *et al.* with a pump source of about 260 mW average power and 45 fs pulse duration at a wavelength of 2350 nm [32]. SC extending in the MIR region was experimentally realized by Guo *et al.* in a Si_3N_4 waveguide where a spectrum ranging from 2500 nm to 4000 nm was obtained when the waveguide was pumped with an optical source of about 110 mW average power and 90 fs pulse duration at a wavelength of 1550 nm [30]. Fang *et al.* [33] presented a Si_3N_4 horizontal slot waveguide with silicon dioxide ($Si0_2$) cladding which was able to produce flat and low normal dispersion. When numerically pumped at 1550 nm wavelength with a 90 kW peak power and 100 fs pulse duration, the waveguide of 5 mm length showed a SC spanning from 504 nm to 4229 nm. Ahmad *et al.* [34] proposed an air clad rectangular waveguide employing stoichiometric Si_3N_4 as core and MgF_2 as the lower cladding. The waveguide was numerically shown to generate a SC spanning from 800 nm to 6500 nm when then the waveguide was pumped with a pulse of 5 kW peak power and 50 fs duration in the anomalous dispersion regime at a wavelength of 1550 nm. With the same pump

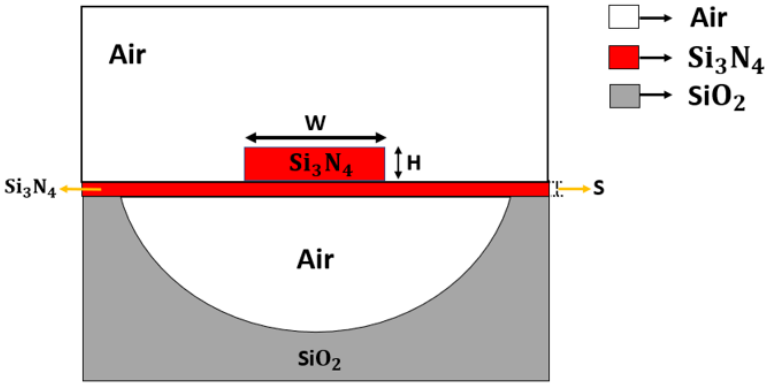

Figure 1: Transverse cross-sectional view of air-clad suspended channel waveguide.

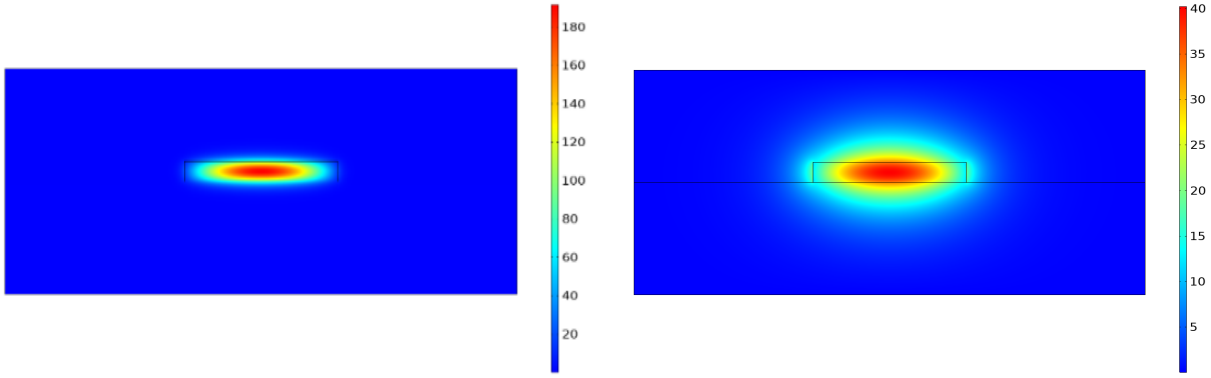

(a) (b)

Figure 2: Mode profile at (a) pump wavelength of 1.55 μm (b) 5 μm for W1= 6 μm and H1= 0.9 μm.

configuration however a SC spanning from 950 nm to 2100 nm was generated in the all normal dispersion regime.

Most of the waveguides discussed above suffer from: lack of pump power availability in practice, fabrication difficulties due to the lattice mismatch between the materials and high propagation losses in terms of integrated photonics. In our work we have tried to overcome these challenges with a good degree of acceptance. We propose a novel suspended core SiN channel waveguide. In this waveguide, the upper cladding is air, while lower cladding is a hollowed-out silica substrate. We numerically generated a SC ranging from 0.8 μm to 6.0 μm with the proposed waveguide at the telecom wavelength. We extensively studied the model with some interesting revelations.

2. Waveguide Design

Figure 1 shows the transverse cross-sectional view of the proposed air-clad suspended channel waveguide (SCW) geometry. The structure consists of Silicon Nitride (Si_3N_4) core suspended on a Si_3N_4 slab. The lower cladding on which the slab rests upon is a hollowed-out Silica (SiO_2) rectangular substrate. SiO_2 cladding is hollowed purposely to introduce air in the cladding which would reduce the cladding losses and provide a better hand from the conventional waveguide designs.

As illustrated in the figure, the core width is denoted as W, core height as H and slab thickness as S. This SCW was designed and simulated in COMSOL Multiphysics software that utilizes the Finite Element Method (FEM) to conduct analysis. After getting a hold on the influence of geometrical parameters on the dispersion and nonlinearity,

we select a waveguide design with particular geometrical parameters for SCG analysis. Figure 2 shows the normalized electric field distribution of the propagating mode in the core at (a) pump wavelength of 1.55 μm and (b) at 5 μm. The waveguide is purposefully designed to support single-mode propagation which is essential for SCG.

3. Theory of Numerical Modeling

The variation of the linear refractive index with wavelength characterizes the material dispersion. The Sellmeier Equation usually adequately explains this variation in refractive index. The Sellmeier Equation for Si_3N_4 [33] is as follows:

$$n^2 = 1 + \frac{3.0249\lambda^2}{\lambda^2 - 0.1353406^2} + \frac{40314\lambda^2}{\lambda^2 - 1239.842^2} \tag{1}$$

where λ is the wavelength in micrometers.

The role of dispersion in SC generation is vital. The dispersion parameter D is commonly used to represent chromatic dispersion and is given as:

$$D(\lambda) = -\frac{\lambda}{c}\frac{d^2 Re(n_{eff})}{d\lambda^2} \tag{2}$$

where c denotes the speed of light and *neff* the effective refractive index [34]. As the respective materials' Sellmeier equations are used, the dispersion parameter embraces both the waveguide and material dispersion. The geometrical variations in the waveguide design are used to achieve dispersion engineering.

The nonlinearity encountered by the waveguide is another important factor for broadband SC [34]. This is addressed by the nonlinear parameter:

$$\gamma = \frac{2\pi n_2}{A_{eff}\lambda} \tag{3}$$

where n_2 is the nonlinear refractive index which and A_{eff} is the effective mode area [34] which is given by:

$$A_{eff} = \frac{(\int\int |F(x,y)|^2 dxdy)^2}{\int\int |F(x,y)|^4 dxdy} \tag{4}$$

where $F(x, y)$ is the modal distribution. High nonlinearity is expected in broadband SC generation. This is usually accomplished by using materials with a high n_2 or by adjusting the waveguide geometry to achieve a lower A_{eff} [35].

The pulse propagation in the optimum dispersion engineered waveguide emphasizes supercontinuum generation. The Generalized Non-linear Schrodinger Equation (GNLSE) quantitatively analyzes SC utilizing the tried-and-true Split Step Fourier Method (SSFM). GNLSE is stated as:

$$\frac{\partial}{\partial z}A(z,T) = -\frac{\alpha}{2}A + \sum_{k\geq 2}^{8}\frac{i^{k+1}}{k!}\beta_k\frac{\partial^k A}{\partial T^k} + i\gamma(|A|^2 A + \frac{i}{\omega_0} + \frac{\partial}{\partial T}(|A|^2 A)) \tag{5}$$

where $A = A(z, T)$ represents the amplitude of the envelope propagating in a retarded time frame $T = t - z/v_g$ at a group velocity $v_g = 1/\beta(\omega_0)$ with a central frequency ω_0, α is the linear propagation loss which is taken to be 0.7 dB/cm, β_k is the $kth - order$ dispersion coefficient obtained using the Taylor expansion of propagation constant $\beta(\omega)$ about the central frequency ω_0 [34]. The Raman contributions have been omitted from the Eq. 5 as reported [36].

In our simulations we have used the hyperbolic secant pulse as the input which is stated as:

$$A(0,T) = \sqrt{P_0}sech(\frac{T}{T_0}) \tag{6}$$

where $T = t - z/v_g(\omega_0)$, T_0 is the input pulse duration, P_0 is the input pulse peak power and v_g is the group velocity at frequency ω_0 [35].

The Finite Element Method (FEM) is used to determine the waveguide's linear properties. This is simply achieved using the inbuilt finite element mode solver provided by the commercially accessible software COMSOL Multiphysics. SC analysis is performed using the well-known computational software MATLAB, which is ideal for complex calculations.

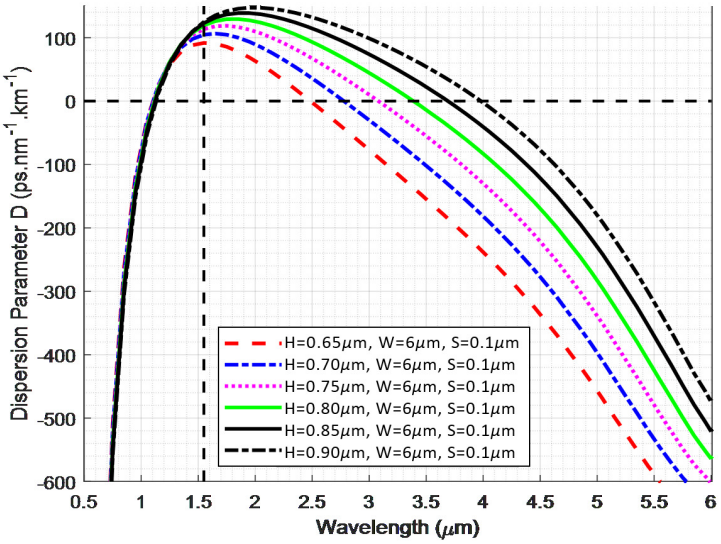

Figure 3: Dispersion characteristics of SCW with a variation in H keeping W and S constant.

Table 1: Dispersion characteristics for a variation in H.

H (μm)	**Dispersion parameter at 1.55 μm (ps.nm^{-1}.km^{-1})**	**Anomalous dispersion regime (μm)**	**Anomalous dispersion bandwidth (μm)**
0.90	125	1.14 – 3.98	2.84
0.85	120	1.13 – 3.69	2.56
0.80	118	1.13 – 3.40	2.27
0.75	110	1.12 – 3.09	1.97
0.70	104	1.11 – 2.86	1.75
0.65	91.7	1.10 – 2.48	1.38

4. Result

4.1. Dispersion characteristics with geometrical variations

Since the geometrical parameters of the waveguide affect the dispersion to great extent, we primarily hold a dispersion analysis with geometrical parameter variations. This analysis also adds value as errors in waveguide fabrication may change the dimensions of the waveguide and having the data on hand can predict probable performance of the waveguide [22]. Figure 3 shows the dispersion profile for a variation in the height of the core, H, from 0.65 μm to 0.9 μm with a step size of 50 nm, with the width of the core, W = 6 μm and slab thickness, S = 0.1 μm being constant. We observe the dispersion characteristics with change in height as this is dominant for our proposed waveguide.

We observe from the Fig. 3 that as H increases, the dispersion parameter increases. We also observe that, the first Zero Dispersion Wavelength (ZDW) at short wavelength relatively remains unchanged whereas the second ZDW shifts towards the long wavelength side as H is increased. At H = 0.90 μm, the dispersion has the highest value of 125 ps.nm^{-1}.km^{-1} with the waveguide offering an anomalous dispersion regime spanning from 1.14 μm to 3.98 μm. At this geometrical parameter, the waveguide offers the highest anomalous dispersion bandwidth of 2.84 μm. At H = 0.65 μm, the dispersion has the lowest value of 91.7 ps.nm^{-1}.km^{-1} with the waveguide offering an anomalous dispersion regime spanning from 1.10 μm to 2.48 μm. At this geometrical parameter, the waveguide offers the lowest anomalous dispersion bandwidth of 1.38 μm. Table 1 summarizes the results obtained for all geometrical variations.

For broadband SCG in general, the ZDW has to be close to the pump wavelength and there should be a wide anomalous dispersion regime offered by the waveguide within a particular limitation. Also the dispersion should be low as possible [34]. At H = 0.90 μm, we observe that a wide anomalous dispersion regime is obtained. But, it is important to note that the dispersion offered is high. At H = 0.65 μm, we observe that the waveguide offers a low dispersion. But, the anomalous dispersion regime is small. It is hard to get all the factors in one place to enhance the SCG. Hence, a trade-off has to done between these factors to achieve the best model for SCG.

4.2. SCG with geometrical variations

Numerical computation of the GNLSE to observe the SC spectra evolution of the different geometrical variations were carried out. Due to its efficiency and accuracy the Split Step Fourier Method (SSFM) was employed by considering 213 grid points at a time step of 2.44 fs. A known factor in producing a broad SC spectrum is the input pulse width, i.e., full width half maximum (TFWHM). Studies show shorter pulses less than 100 fs, when used generate a broad spectrum [35]. Ultrashort laser pulses (pulse width = 50 fs, peak power: 1 kW – 20 kW, pulse type: hyperbolic secant) were launched into the proposed 5 mm optical waveguide. Higher order dispersion terms up to the 8th order were incorporated into the numerical simulation for spurious free SC spectral broadening [35]. Wavelength dependent mode effective areas and the corresponding non-linear coefficients were calculated at pump wavelength.

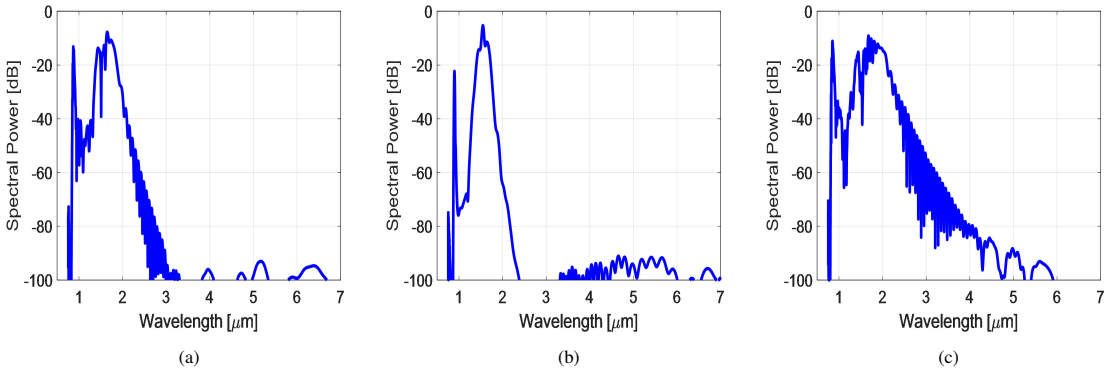

Figure 4: SC Spectra at peak powers of (a) 5 kW (b) 10 kW (c) 20 kW at pump wavelength of 1.55 μm for Structure Parameters W= 6.0 μm and H=0.90 μm.

Figure 4 and 5 shows the SC spectra and the corresponding spectral and temporal evolution for the geometrical parameters: W= 6.0 μm and H= 0.90 μm. At a peak power of 5 kW, we see a spectrum ranging from 0.9 μm to 1.9 μm within the -30 dB power level from the peak. However, there is a gradual decline in the spectral curve, without any fluctuations. Increasing power to 10 kW barely increases SC as we get a spectrum ranging from 0.9 μm to 2 μm. A gradual decline in the SC is observed with considerable fluctuations. Heavy distortion in the spectrum is observed when power is raised to 20 kW, with spectrum extending up to 2.5 μm.

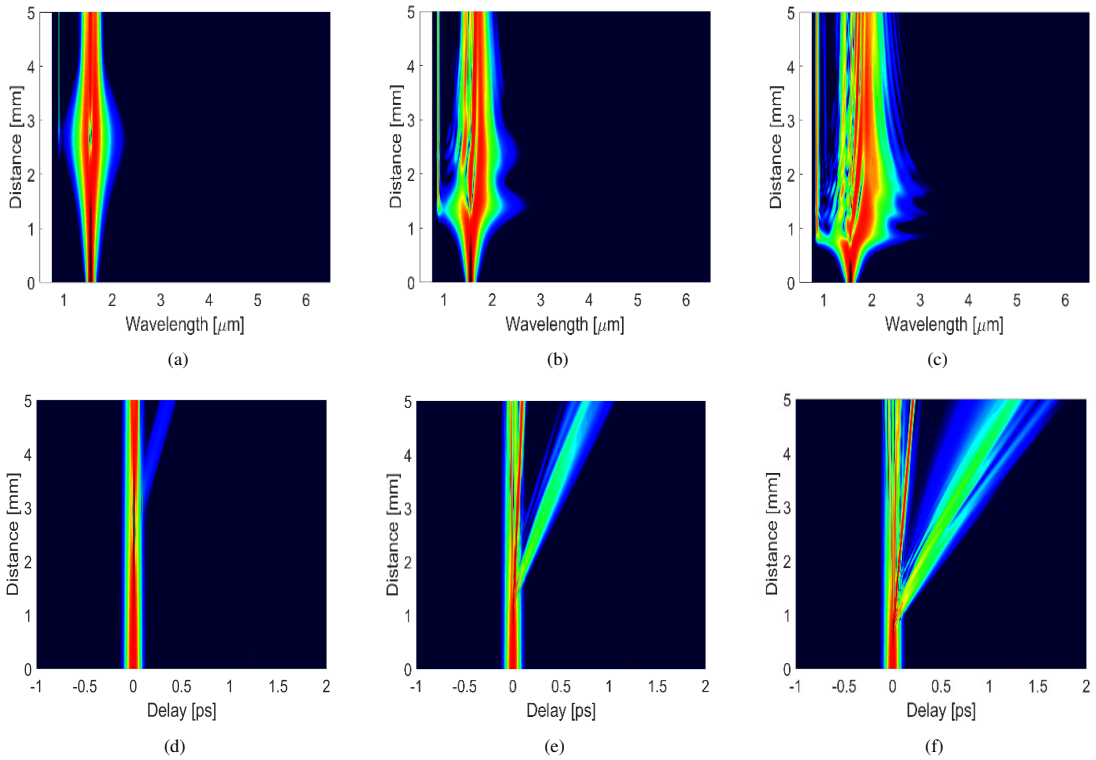

Figure 5: The spectral (top) and temporal (bottom) density evolutions in 1^{st}, 2^{nd} and 3^{rd} column plotted at 1.55 μm pump wavelength corresponding to Figs. 4 (a)–(c), respectively.

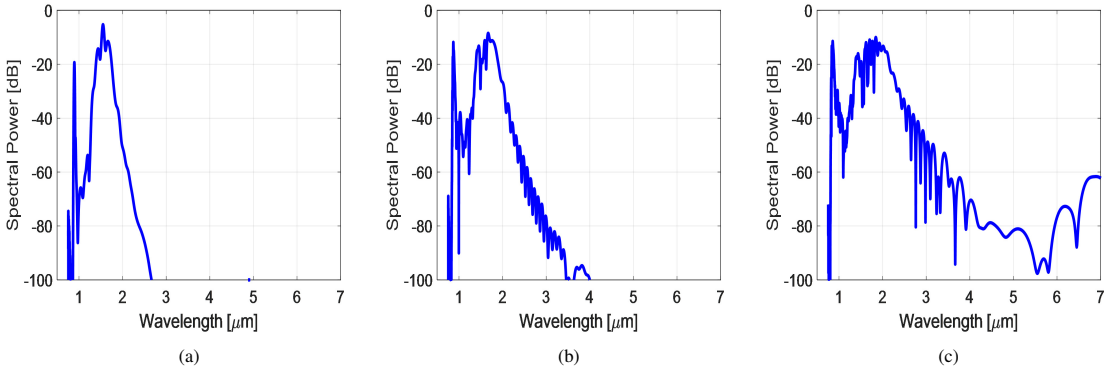

Figure 6: SC Spectra at peak powers of (a) 5 kW (b) 10 kW (c) 20 kW at pump wavelength of 1.55 μm for Structure Parameters W= 6.0 μm and H=0.80 μm.

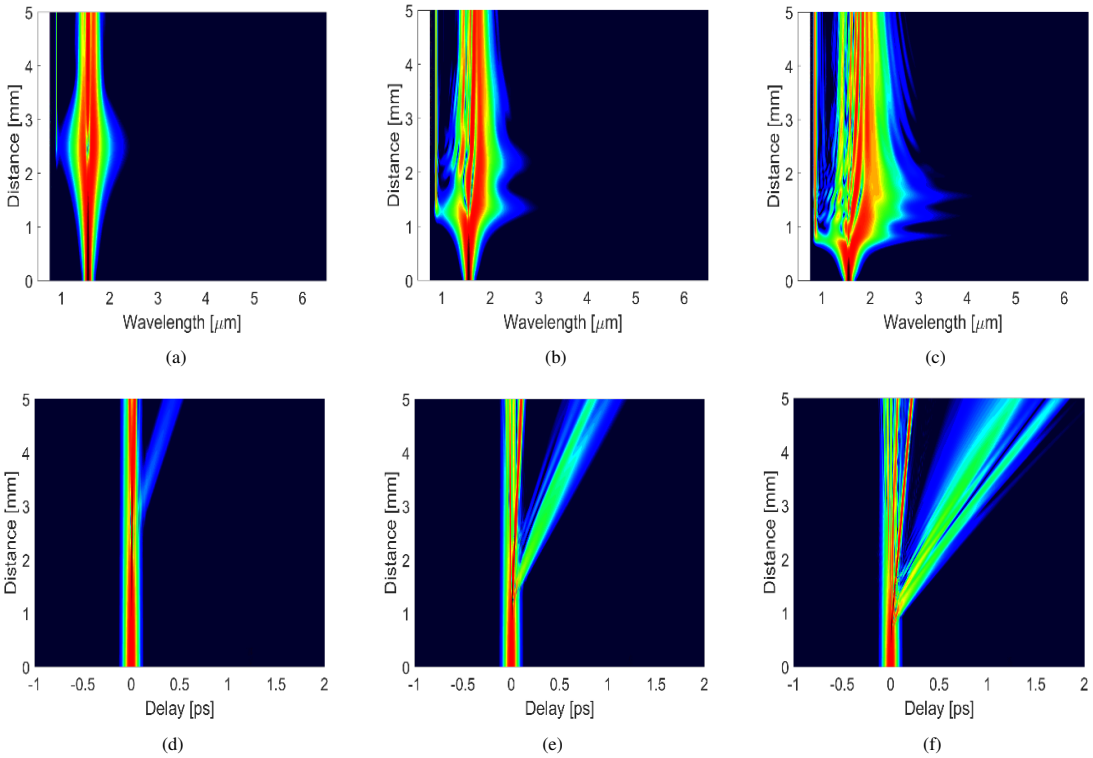

Figure 7: The spectral (top) and temporal (bottom) density evolutions in 1^{st}, 2^{nd} and 3^{rd} column plotted at 1.55 µm pump wavelength corresponding to Figs. 6 (a)–(c), respectively.

Figure 6 and 7 shows the SC spectra and the corresponding spectral and temporal evolution for the geometrical parameters: W= 6.0 µm and H= 0.80 µm. At a peak power of 5 kW, we see a spectrum ranging from 1.0 µm to 2 µm within the -30 dB power level from the peak. However, there is a gradual decline in the spectral curve, without any fluctuations. Increasing power to 10 kW barely increases SC as we get a spectrum ranging from 1 µm to 2.1 µm. A gradual decline is also observed here with considerable fluctuations. Heavy distortion in the spectrum is observed when power is raised to 20 kW, with spectrum increasing up to 2.7 µm.

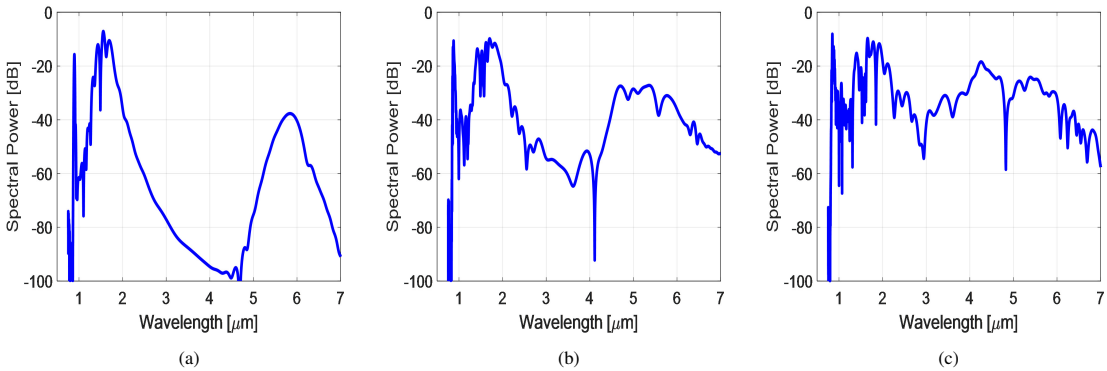

Figure 8: SC Spectra at peak powers of (a) 5 kW (b) 10 kW (c) 20 kW at pump wavelength of 1.55 µm for Structure Parameters W= 6.0 µm and H=0.70 µm.

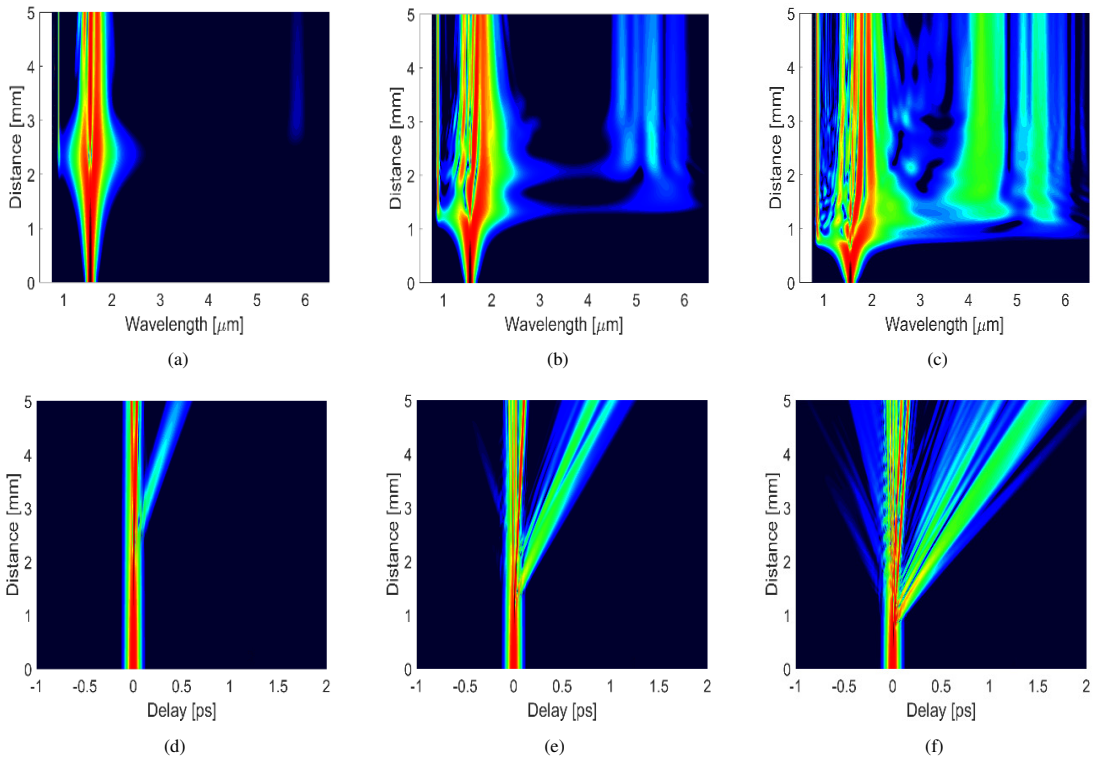

Figure 9: The spectral (top) and temporal (bottom) density evolutions in 1^{st}, 2^{nd} and 3^{rd} column plotted at 1.55 μm pump wavelength corresponding to Figs. 8 (a)–(c), respectively.

Figure 8 and 9 shows the SC spectra and the corresponding spectral and temporal evolution for the geometrical parameters: W= 6.0 μm and H= 0.70 μm. At a peak power of 5 kW, we obtain a SC with a significant dip between 2 μm and 5.8 μm which falls well below -30 dB power level. As power is increased to 10 kW, spectral components improve around the dip region. At peak power of 20 kW there is still fluctuations in the power level, where spectral component falls below -30 dB power level, resulting in the curve not being flat. Although, it produces a spectrum ranging from 0.9 μm to 6 μm at 20 kW, the instability of the spectrum makes it less desirable for practical applications.

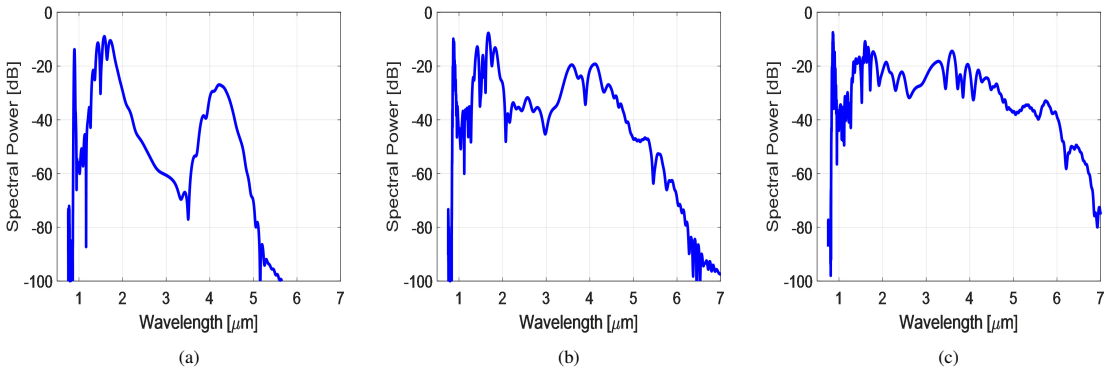

Figure 10: SC Spectra at peak powers of (a) 5 kW (b) 10 kW (c) 20 kW at pump wavelength of 1.55 μm for Structure Parameters W= 6.0 μm and H=0.65 μm.

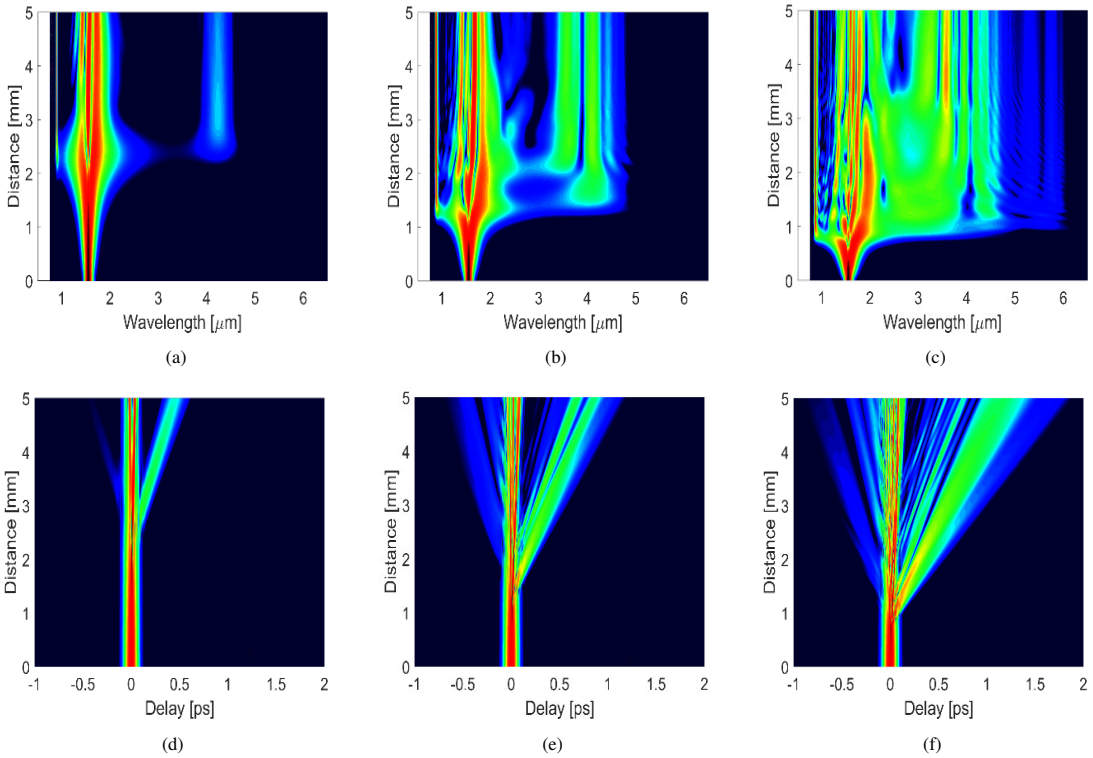

Figure 11: The spectral (top) and temporal (bottom) density evolutions in 1^{st}, 2^{nd} and 3^{rd} column plotted at 1.55 μm pump wavelength corresponding to Figs. 10 (a)–(c), respectively.

Figure 10 and 11 shows the SC spectra and the corresponding spectral and temporal evolution for the geometrical parameters, W= 6.0 μm and H= 0.65 μm. At peak power of 5 kW, there is a considerable dip in the SC spectrum between 2 μm to 4 μm. Further increase in peak power to 10 kW improves the spectral components around the dip region. At 20 kW, a SC spectrum spanning from 0.8 μm to 6 μm which falls in the MIR is observed with good flatness within the -30 dB power level from the peak. When peak powers of more than 20 kW were applied, no further improvement in the SC spectra was observed.

4.3. Proposed SCG model

After observing the dispersion characteristics and also conducting a SCG analysis on all possible geometrical variations of the waveguide, we propose the optimized model with the related geometrical parameters. The parameters of the proposed model is depicted in the Table 2.

Table 2: Geometrical parameters and characteristics of the proposed waveguide

Height (μm)	**Width (μm)**	**Thickness (μm)**	**Dispersion parameter at 1.55 μm (ps.nm−1.km−1)**	**Nonlinear parameter at 1.55 μm ($W^{-1}.km^{-1}$)**	**Effective mode area at 1.55 μm ($μm^2$)**
0.65	6.00	0.1	91.7	0.34	2.96

At H = 0.65 μm, the waveguide offers a dispersion of 91.76 $ps.nm^{-1}.km^{-1}$ at the pump wavelength (1.55 μm) with an anomalous dispersion regime spanning from 1.10 μm to 2.48 μm. Figure 12 shows the change in nonlinear parameter and effective mode area with wavelength for the proposed model where the mode effective area is 2.96

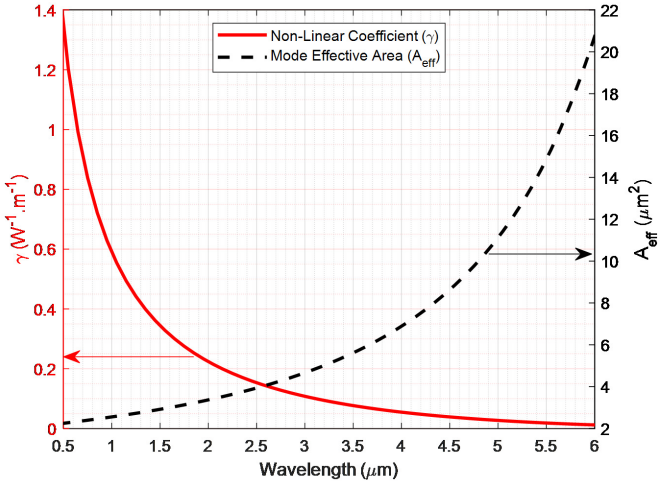

Figure 12: Effective mode area and nonlinear parameter variation with change in wavelength for H = 0.65 μm.

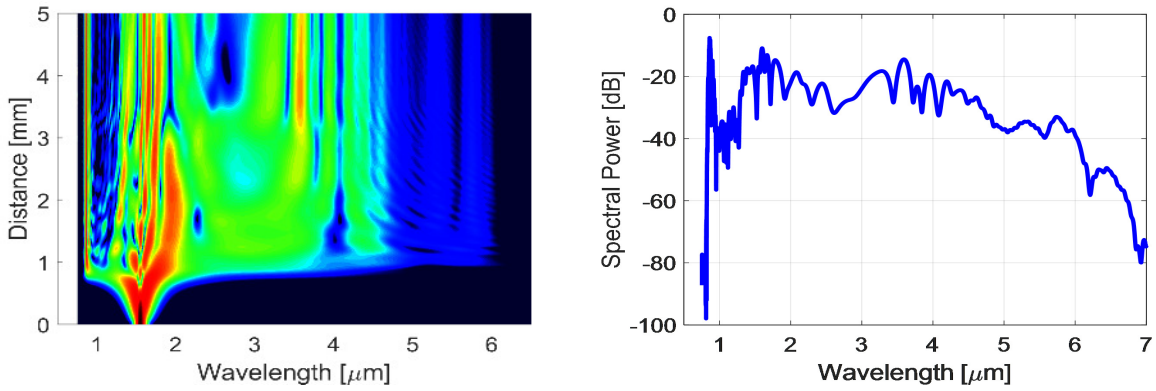

(a) (b)

Figure 13: (a) Spectral density plot (b) SC spectra of the waveguide at H = 0.65 μm, W = 0.6 μm and S = 0.1 μm with a pump of 50 fs, 20kW configuration at 1.55 μm.

μm^2 and the non-linear parameter is 0.34 $W^{-}1.m^{-1}$ at the pump wavelength. The nonlinearity is relatively high and the effective mode area and dispersion are low which is desired for broadband SCG [34]. Hence, at geometrical parameters of H = 0.65 μm, W = 6 μm and S = 0.1 μm, the waveguide showcases characteristics which are required for broadband SCG. Figure 13 shows the SC spectra and corresponding spectral evolution of the proposed model where the waveguide is pumped with a 50 fs, 20 kW pulse at the telecom wavelength (1.55 μm).

From Fig. 13, we observe that a broad spectrum ranging from 0.8 μm to 6 μm is obtained with the necessary pump configuration at the telecom wavelength. A broadband SCG is obtained due to the trade-off between the linear and nonlinear effects. Regarding the spectral broadening, it is primarily governed by Self-Phase Modulation (SPM) [11] during the first 1.5 μm propagation by the pulse. At 1.5 μm propagation length, the soliton dynamics comes into play. The fundamental soliton during propagation breaks up into smaller solitons which shifts towards the long wavelength side [22]. Also, two dispersive waves are generated in the short and long wavelength side of the spectrum due to the presence of two ZDW in its corresponding dispersion curve [34]. The peak of the first dispersive wave is observed at about 1 μm and center of the second dispersive wave located at about 4 μm. These dispersive waves contribute to the spectral broadening of the pulse. It is also noteworthy that the waveguide showcased an anomalous dispersion region which was not too big. Long anomalous dispersion could often reduce the power of the soliton as it travels which

would result in a reduction in the energy transformation of the soliton to the dispersive wave leading to reduced SCG. Our waveguide uses showcases a dispersion profile which keeps a trade-off to balance all the factors responsible for broadband SCG. Hence, a broadband SC is obtained due to the contribution of the linear and nonlinear effects within the waveguide.

The proposed Si3N4 channel waveguide can be fabricated as similar waveguides were achieved as reported [37]. The core substrate can be usually deposited using the mature fabrication techniques such as Low Pressure Chemical Vapor Depositon (LPCVD) [38, 39] and Plasma-Enhanced Chemical Vapor Deposition (PEVCD) [40]. The hollow cladding region can be realized using wafer bonding [41, 42], wet etching [37, 43] and the micromachining and nanomachining techniques [44].

5. Conclusion

The proposed 5 mm long on-chip CMOS compatible suspended core Silicon Nitride (SiN) channel waveguide is proposed. The rectangular core is suspended on a Silicon Nitride slab of thickness 0.1 μm. The upper cladding is air, while the lower cladding is a hollowed-out silica substrate. Complex microstructure such as this is now possible due to the advancement of fabrication techniques. The dispersion profile for a number of geometrical variations were studied, where for the width of the core, W = 0.6 μm, height of the core, H = 0.65 μm and slab thickness, S = 0.1 μm, provided a fairly flat anomalous dispersion with sound span of the anomalous dispersion regime. Dispersion parameter of 91.76 $ps.nm^{-1}.km^{-1}$ at pump wavelength is observed, while the range of anomalous dispersion region where non-linear effects take place is observed between 1.10 μm to 2.48 μm.

The proposed waveguide was numerically analyzed for SCG. By solving the GNLSE, the 5 mm waveguide was pumped with a pulse of duration 50 fs and peak power varying from 5 kW to 20 kW. This study was performed by varying the height of the core, H of the waveguide from 0.65 μm to 0.90 μm, while W = 0.60 μm and S = 0.1 μm were kept constant. SC generation at a core height of 0.65 μm produced a flat spectrum from 0.8 μm to 6 μm at peak power of 20 kW within the -30 dB power level. At H = 0.70 μm, similar SC was achieved with fluctuations in the spectrum. Core height of 0.80 μm and 0.90 μm yielded spectrum less than 3 μm. Hence the broadband SC of 0.8 μm to 6 μm was produced with geometrical parameters of H = 0.65 μm, W = 0.60 μm and S = 0.1 μm when the waveguide was pumped with a pulse of duration 50 fs and 20 kW peak power at the telecom wavelength (1.55 μm). Flatness in the spectral curve and with other advantages of Silicon Nitride such as negligible Raman Effect and TPA, this waveguide as a modified optical source will be an asset in the industry of gas sensing, food quality control and bio-medical imaging.

References

[1] D. Grassani, E. Tagkoudi, H. Guo, C. Herkommer, F. Yang, T. J. Kippenberg, C.-S. Bres, Mid infrared gas spectroscopy using efficient fiber laser driven photonic chip-based supercontinuum, Nature Communications 10 (2019) 97–111.

[2] N. M. Israelsen, C. R. Petersen, A. Barh, D. Jain, M. Jensen, G. Hannesschläger, P. Tidemand-Lichtenberg, C. Pedersen, A. Podoleanu, O. Bang, Real-time high-resolution mid-infrared optical coherence tomography, Light: Science 8 (2019).

[3] C. Ware1, S. Cordette, C. Lepers, I. Fsaifes, B. Kibler, C. Finot, GuyMillot, Spectral Slicing of a Supercontinuum Source for WDM/DS-OCDMA Application, 2008 10th Anniversary International Conference on Transparent Optical Networks (2008) 158–161.

[4] J. X. Zhang, K. Hoshino, Optical transducers: Optical molecular sensing and spectroscopy, Molecular Sensors and Nanodevices: Principles (2018).

[5] S. K. Selvaraja, P. Sethi, Review on Optical Waveguides, Emerging Waveguide Technology (2018).

[6] Z. Hui, L. Zhang, W. Zhang, CMOS compatible on-chip telecom-band to mid-infrared supercontinuum generation in dispersion-engineered reverse strip/slot hybrid Si_3N_4 waveguide, Journal of Modern Optics 65 (2017) 1–11.

[7] A. D. Torre, M. Sinobad, R. Armand, B. Luther-Davies, P. Ma, S. Madden, A. Mitchell, D. J. Moss, J.-M. Hartmann, V. Reboud, J.-M. Fedeli, C. Monat, C. Grillet, Mid-infrared supercontinuum generation in a low-loss germanium-on-silicon waveguide, APL Photonics 6 (2021).

[8] H. Hu, X. Zhang, W. Li, N. K. Dutta, Simulation of octave spanning mid-infrared supercontinuum generation in dispersion-varying planar waveguides, Applied Optics 54 (2015) 3448–3454.

[9] C. R. Phillips, C. Langrock, J. S. Pelc, M. M. Fejer, J. Jiang, M. E. Fermann, I. Hartl, Supercontinuum generation in quasi-phase-matched $LiNbO_3$ waveguide pumped by a Tm-doped fiber laser system, Optics Letters 36 (2011).

[10] Y. Yu, X. Gai, P. Ma, D.-Y. Choi, Z. Yang, R. Wang, S. Debbarma, S. J. Madden, , B. Luther-Davies, A broadband, quasi-continuous, mid-infrared supercontinuum generated in a chalcogenide glass waveguide, Laser & Photonics Reviews 8 (2014) 792–798.

[11] M. R. Karim, B. M. A. Rahman, Ultra-broadband mid-infrared supercontinuum generation using chalcogenide rib waveguide, Optical and Quantum Electronics 48 (2016).

[12] T. S. Saini, U. K. Tiwari, R. K. Sinha, Rib waveguide in Ga-Sb-S chalcogenide glass for on-chip mid-IR supercontinuum sources: Design and analysis, Journal of Applied Physics 122 (2017).
[13] N. Singh, M. X. snd D. Vermeulen, K. Shtyrkova, N. Li, P. Callahan, E. Magden, A. Ruocco, N. M. Fahrenkopf, C. Baiocco, B. Kuo, S. Radic, E. Ippen, F. Kärtner, M. Watts, Octave-spanning coherent supercontinuum generation in silicon on insulator from 1.06 μm to beyond 2.4 μm, Light: Science & Applications 07 (2018) 17131.
[14] R. Lau, M. Lamont, A. Griffith, Y. Okawachi, M. Lipson, A. Gaeta, Octave-spanning mid-infrared supercontinuum generation in silicon nanowaveguides, Optics Letters 39 (2014) 4518–4521.
[15] N. Singh, D. D. Hudson, Y. Yu, C. Grillet, S. D. Jackson, A. Casas-Bedoya, A. Read, P. Atanackovic, S. G. Duvall, S. Palomba, B. Luther-Davies, S. Madden, D. J. Moss, B. J. Eggleton, Midinfrared supercontinuum generation from 2 to 6 μm in a silicon nanowire, Optica 2 (2015) 797–802.
[16] N. Nader, D. L. Maser, F. C. Cruz, A. Kowligy, H. Timmers, J. Chiles, C. Fredrick, D. A. Westly, S. W. Nam, R. P. Mirin, J. M. Shainline, S. Diddams, Versatile silicon-waveguide supercontinuum for coherent mid-infrared spectroscopy, APL Photonics 3 (2018).
[17] L. Zhang, A. M. Agarwal, L. C. Kimerling, J. Michel, Nonlinear Group IV photonics based on silicon and germanium: from near-infrared to mid-infrared, Nanophotonics 3 (2014) 247–268.
[18] A. D. Torre, M. Sinobad, R. Armand, B. Luther-Davies, P. Ma, S. Madden, A. Mitchell, D. J. Moss, J.-M. Hartmann, V. Reboud, J.-M. Fedeli, C. Monat, , C. Grillet, Mid-infrared supercontinuum generation in a low-loss germanium-on-silicon waveguide, APL Photonics 6 (2021).
[19] M. Sinobad, A. DellaTorre, R. Armand, B. Luther-Davies, P. Ma, S. Madden, A. Mitchell, D. J. Moss, J.-M. Hartmann, J.-M. Fedeli, C. Monat, C. Grillet, Mid-infrared supercontinuum generation in silicon-germanium all-normal dispersion waveguides, Optics Letters 45 (2020) 5008–5011.
[20] R. Baets, A. Z. Subramanian, S. Clemmen, B. Kuyken, P. Bienstman, N. L. Thomas, G. Roelkens, D. V. Thourhout, P. Helin, S. Severi, Silicon photonics: Silicon nitride versus silicon-on-insulator, 2016 Optical Fiber Communications Conference and Exhibition (2016) 1–3.
[21] Q. Wilmart, H. E. Dirani, N. Tyler, D. Fowler, S. Malhouitre, S. García, M. Casale, S. Kerdiles, K. Hassan, C. Monat, X. Letartre, A. Kamel, M. Pu, K. Yvind, L. Oxenlowe, W. Rabaud, C. Sciancalepore, B. Szelag, S. Olivier, A Versatile Silicon-Silicon Nitride Photonics Platform for Enhanced Functionalities and Applications, Applied Sciences 09 (2019) 255.
[22] R. Sharma, S. Kaur, P. Chauhan, A. Kumar, Computational design & analysis of $GeSe_2$-As_2Se_3-PbSe based rib waveguide for mid-infrared supercontinuum generation, Optik 220 (2020).
[23] C. Lafforgue, S. Guerber, J. M. Ramirez, G. Marcaud, C. Alonso-Ramos, X. L. Roux, D. Marris-Morini, E. Cassan, C. Baudot, F. Boeuf, S. Cremer, S. Monfray, L. Vivien, Broadband supercontinuum generation in nitrogen-rich silicon nitride waveguides using a 300 mm industrial platform, Photonics Research 8 (2020) 352–358.
[24] S. T. Ilie, T. D. Bucio, T. Rutirawut, L. Mastronardi, I. Skandalos, H. Chong, F. Y. Gardes, Silicon-rich silicon nitride CMOS platform for integrated optical phased arrays, Proc. SPIE 11690 (2021) 1169005–9.
[25] D. J. Blumenthal, R. Heideman, D. Geuzebroek, A. Leinse, C. Roeloffzen, Silicon Nitride in Silicon Photonics, Proceedings of the IEEE 106 (2018) 2209–2231.
[26] H. Zhao, B. Kuyken, S. Clemmen, F. Leo, A. Subramanian, A. Dhakal, P. Helin, S. Severi, E. Brainis, G. Roelkens, R. Baets, Visible-to-near-infrared octave spanning supercontinuum generation in a silicon nitride waveguide, Optics Letters 40 (2015) 2177–2180.
[27] A. R. Johnson, A. S. Mayer, A. Klenner, K. Luke, E. S. Lamb, M. R. E. Lamont, C. Joshi, Y. Okawachi, F. W. Wise, M. Lipson, U. Keller, A. L. Gaeta, Octave-spanning coherent supercontinuum generation in a silicon nitride waveguide, Optics Letters 40 (2015) 5117–5120.
[28] M. P. Xing Liu, B. Zhou, C. J. Krückel, A. Fülöp, V. Torres-Company, M. Bache, Octave-spanning supercontinuum generation in a silicon-rich nitride waveguide, Optics Letters 41 (2016) 2719–2722.
[29] M. Porcel, F. Schepers, J. Epping, T. Hellwig, M. Hoekman, R. Heideman, P. van der Slot, C. Lee, R. Schmidt, R. Bratschitsch, C. Fallnich, K. Boller, Two-octave spanning supercontinuum generation in stoichiometric silicon nitride waveguides pumped at telecom wavelengths, Optics Express 25 (2017) 1542–1554.
[30] H. Guo, C. Herkommer, A. Billat, D. Grassani, C. Zhang, M. H. P. Pfeiffer, W. Weng, C.-S. Brès, T. J. Kippenberg, Mid-infrared frequency comb via coherent dispersive wave generation in silicon nitride nanophotonic waveguides, Nature Photonics 12 (2018) 330–335.
[31] D. Grassani, A. Billat, M. H. P. Pfeiffer, H. Guo, T. North, T. J. Kippenberg, C. Brès, Mid-infrared supercontinuum generation in a SiN waveguide pumped at 1.55 micron, Frontiers in Optics (2016).
[32] D. Martyshkin, V. Fedorov, T. Kesterson, S. Vasilyev, H. Guo, J. Liu, W. Weng, K. Vodopyanov, T. Kippenberg, S. Mirov, Visible-near-middle infrared spanning supercontinuum generation in a silicon nitride (Si_3N_4) waveguide, Optical Material Express 09 (2019) 2553–2559.
[33] Y. Fang, C. Bao, Z. Wang, B. Liu, L. Zhang, X. Han, Y. He, H. Huang, Y. Ren, Z. Pan, Y. Yue, Three-Octave Supercontinuum Generation Using SiO_2 Cladded Si_3N_4 Slot Waveguide With All-Normal Dispersion, Journal of Lightwave Technology 38 (2020) 3431–3438.
[34] H. Ahmad, M. R. Karim, B. M. A. Rahman, Dispersion-engineered silicon nitride waveguides for mid-infrared supercontinuum generation covering the wavelength range 0.8-6.5 μm, Laser Physics 29 (2019) 025301.
[35] T. S. Saini, A. Kumar, R. K. Sinha, Design and modelling of dispersion-engineered rib waveguide for ultra broadband mid-infrared supercontinuum generation, Journal of Modern Optics 64 (2016) 1–7.
[36] M. Karpov, H. Guo, A. Kordts, V. Brasch, M. H. Pfeiffer, M. Zervas, M. Geiselmann, T. J. Kippenberg, Raman Self-Frequency Shift of Dissipative Kerr Solitons in an Optical Microresonator, Physical Review Letters 116 (2016).
[37] T. H. Rai Kou, J. Horng, J.-H. Kang, Y. Wang, X. Zhang, F. Wang, Mid-IR broadband supercontinuum generation from a suspended silicon waveguide, Optics Letters 43 (2018) 1387–1390.
[38] Y. Wang, V. Pelgrin, S. Gyger, G. M. Uddin, X. Bai, C. Lafforgue, L. Vivien, K. D. Jöns, E. Cassan, Z. Sun, Enhancing Si_3N_4 Waveguide Nonlinearity with Heterogeneous Integration of Few-Layer WS_2, ACS Photonics 8 (2021) 2713–2721.
[39] Daldosso, Nicola, M. Melchiorri, F. Riboli, M. Girardini, G. Pucker, M. Crivellari, P. Bellutti, A. Lui, L. Pavesi, Design, fabrication, structural and optical characterization of thin Si_3N_4 waveguides, IEEE J. Lightwave Technol 22 (2004) 1734.
[40] A. Gorin, A. Jaouad, E. Grondin, V. Aimez, P. Charette, Fabrication of silicon nitride waveguides for visible-light using PECVD: a study of the effect of plasma frequency on optical properties, Optics Express 16 (2008) 13509–13516.
[41] N. Nader, A. Kowligy, J. Chiles, E. J. Stanton, H. Timmers, A. J. Lind, F. C. Cruz, D. M. B. Lesko, K. A. Briggman, S. W. Nam, S. A.

Diddams, R. P. Mirin, Infrared frequency comb generation and spectroscopy with suspended silicon nanophotonic waveguides, Optica 6 (2019) 1269–1276.
[42] J. Chiles, S. Khan, J. Ma, S. Fathpour, High-contrast, all-silicon waveguiding platform for ultra-broadband mid-infrared photonics, Applied Physics Letters 103 (2013) 151106.
[43] Y. Xia, C. Qiu, X. Zhang, W. Gao, J. Shu, Q. Xu, Suspended Si ring resonator for mid-IR application, Optics Letters 38 (2013) 1122–1124.
[44] T. H. Stievater, M. W. Pruessner, W. S. Rabinovich, D. Park, R. Mahon, D. A. Kozak, J. B. Boos, S. A. Holmstrom, J. B. Khurgin, Suspended photonic waveguide devices, Applied Optics 54 (2015) F164–F173.